Applied Physics Letters

Photonics-inspired terahertz whispering gallery mode resonator waveguide on silicon platform

Cite as: Appl. Phys. Lett. **119**, 171103 (2021); https://doi.org/10.1063/5.0065696
Submitted: 04 August 2021 • Accepted: 11 October 2021 • Published Online: 25 October 2021

Shuyu Zhou, Xuecou Tu, Qiangqiang Wu, et al.

Applied Physics Letters ARTICLE scitation.org/journal/apl

Photonics-inspired terahertz whispering gallery mode resonator waveguide on silicon platform

Cite as: Appl. Phys. Lett. **119**, 171103 (2021); doi: 10.1063/5.0065696
Submitted: 4 August 2021 · Accepted: 11 October 2021 ·
Published Online: 25 October 2021

Shuyu Zhou,[1] Xuecou Tu,[1,2,a)] Qiangqiang Wu,[1] Mengxin Liu,[1,2] Yichen Zhang,[1] Pengfei Chen,[1] Wohu Wang,[1] Yucheng Xu,[1] Jianqin Deng,[3] Qingyuan Zhao,[1,2] Xiaoqing Jia,[1,2] Labao Zhang,[1,2] Lin Kang,[1,2] Jian Chen,[1,2] and Peiheng Wu[1,2]

AFFILIATIONS

[1]Research Institute of Superconductor Electronics (RISE), School of Electronic Science and Engineering, Nanjing University, Nanjing 210023, China
[2]Purple Mountain Laboratories, Nanjing 211111, China
[3]41st Research Institute of CETC, Qingdao, China

[a)]Author to whom correspondence should be addressed: tuxuecou@nju.edu.cn

ABSTRACT

Terahertz (THz) photonic waveguides are of great importance in THz integrated technology, especially for versatile signal processing. However, in THz photonics, very few fundamental "building blocks" equivalent to those used in muti-functional electronics circuits exist. This study proposes a photonics-inspired micro-ring whispering gallery mode resonator (WGMR) waveguide with a standard waveguide-compatible package on silicon platform. A gradual taper is integrated on the same chip to improve the coupling efficiency and reduce transmission loss. The packaged WGMR waveguide with an operating range of 0.360 to 0.440 THz had a maximum measured extinction ratio of 32 dB at 0.390 THz, with a Q factor of 385 and an insertion loss of 2.6 dB. The compact and standard waveguide-compatible packaged WGMR can easily be integrated into practical terahertz application systems for THz signal processing and as a tool for the study of fundamental THz science.

In the past decade, there has been a significant surge of progress in enabling integrated, compact, and efficient chip-scale THz technology, which could bridge the THz gap in meaningful ways.[1–4] Silicon-based integrated technology provides a platform for massive integration, micro-package in hybrid THz microsystems.[5–11] In addition to offering low-loss propagation of THz signals, silicon-based photonic-inspired structures can provide additional passive functionality and are creating significant interest in THz waveguides.[12–15] The conductor loss of a THz signal in the metal waveguide increases with an increase in frequency, resulting in a larger electromagnetic power attenuation.[16] When the frequency is above 1 THz, the width of the rectangular metal waveguide is smaller than 250 μm, reaching the limit of mechanical treatment accuracy.[17,18] Therefore, metal waveguides are generally used in devices with frequencies below 1 THz. In addition, metal waveguides are not easily integrated with THz photonic components and THz fibers, including tube-tube fibers and solid-core hollow-core photonic bandgaps.[19] These waveguides can provide a number of options for versatile signal processing with low-dispersion. However, these have the disadvantages of high fiber interface loss or difficult integration. Much work needs to be done to enable fully functional THz waveguides and integrated devices in the same substrate.

The whispering gallery mode resonators (WGMRs) have been explored in numerous applications at optical frequency range due to its small mode volume and excellent signal processing capability.[20–24] Photonics-inspired research on WGMRs in the THz domain is just at its infancy with a huge potential for THz photonic devices.[25–34] Whispering gallery mode (WGM) cavity for terahertz pulses was first reported by D. Grischkowsky in 2003.[25] It promoted the development of Terahertz Science and technology, especially in the interaction between the terahertz pulse and dielectric resonator. In this pioneering work, the resonator and coupling waveguide are discrete, the input and output adopt free space coupling, the efficiency is still relatively low, and the alignment of components is very difficult. In 2019, Zhang *et al.* developed a micro-ring using a Teflon material coupled with optical fiber to analyze the conditions of the excitation of multi-mode WGM[26,27] and discussed the phenomenon of Fano resonance in the WGMR.[28] Vogt *et al.* focused on fiber-coupled WGM, high-resistance silicon balls,[29] quartz bubbles,[30] and silicon disks.[31] These studies

opened the way for the use of a WGMR in the field of integrated THz photonic technology. Notably, the resonant characteristics of these devices were severely affected by micro-assembly, the THz signals deliver through the discrete fiber for input and output, and this hinders the large-scale integration of THz photonic devices. Existing research has generally produced high-order mode and high loss up to 6 dB or more.[26,33] Efficient coupling strategy is not yet well established, and still, many open questions remain about implementation and optimization. Furthermore, if the waveguide and the WGMR resonator can be integrated on a chip, like an optical band, the complexity of the system will be reduced, which would greatly promote the research of THz devices on a chip. A package for THz device chips using standard rectangular metal waveguides is desirable for the input and output interfaces of THz waves.

In this Letter, a WGMR waveguide chip on a silicon platform with compact and standard waveguide-compatible packages is demonstrated. To alleviate the difficulty of the deep silicon etching preparation process, a symmetrical dual micro-ring structure is adopted. A gradual taper structure is adopted in the same chip to solve the coupling problem between the metal and dielectric resonator waveguides.[8–10,35–37] A stable Q factor, high extinction ratio, and wide working range of the WGMR waveguide on a silicon chip were obtained under the synergistic action of these two structures. The WGMR waveguide overcomes the losses associated with interconnects over waveguide ports, leveraging the low loss and extinction ratio of the dielectric waveguide and demonstrated a common platform for the implementation of terahertz WGM-integrated systems.

The theory of electromagnetic coupling of the micro-ring WGMR structures can be found in many studies.[38,39] The design of the dual micro-ring WGMR waveguide made by the high resistivity float zone silicon (HRFZ-Si) (refractive index 3.4174)[40] chip is shown in Fig. 1(a). The selection of low-loss materials is the key to achieving a high Q THz WGMR since most materials have strong absorption at THz.[38,40] The micro-ring radius r is defined as half of the sum of the outer diameter and inner diameter, the gap g is defined as the distance between the micro-ring and the straight waveguide, the micro-ring's width w is defined as the difference between the outer diameter and the inner diameter of the micro-ring, and width of the straight waveguide is also w. The heights of the substrate and micro-ring are h_1 and h_2, respectively, and the upper and lower layers are air. The lower right corner shows the cross section of the straight waveguide in the WGMR, where h_1 is the thickness of the substrate, h_2 is the height of the rib waveguide, $h_1 = 60\,\mu$m, $h_2 = 140\,\mu$m. When the heights h_1 and h_2 are determined, the effective refractive index method is used to calculate the effective refractive index of the section. Owing to the principle of WGM, when the value of width w reaches a certain value, it may trigger the higher order radial mode. Therefore, we set w to 210 μm, and the calculated effective refractive index n_{eff} was equal to 2.65. The micro-ring radius was set as 1820 μm, so the free spectral range (FSR) was 6.5 GHz according to Eq. (1), where m is the mode number of WGM.

$$FSR = 2\pi r n_{eff}[1/(m+1) - 1/m]. \quad (1)$$

To improve the Q and extinction ratio of the WGMR, it is usually necessary to make a very small distance between the WGMR and the bus waveguide [labeled g in Fig. 1(a)]. In the waveguide chip fabrication, when the gap is 4 μm, it is very difficult to etch silicon at 140 μm depth, and the etching error is troublesome. Through analysis and calculation, it is found that the dual rings ($g = 18\,\mu$m) can be used to achieve the same resonance characteristics as the single ones ($g = 4\,\mu$m). To demonstrate the advance, the transmissions of dual and single ring WGMR waveguides with the same micro-ring size but different g were calculated for comparison. In the upper Fig. 1(b), the black and pink curves are the calculated transmissions for the single ring WGMR waveguide with $g = 4\,\mu$m and the dual micro-ring ones with $g = 18\,\mu$m, respectively. TE (36, 36, 1) (hereafter abbreviated as TE36), TE (39, 39, 1) (TE39), and TE (45, 45, 1) (TE45) are the mode numbers of corresponding WGM modes in the sphere. The calculated Q factors are 254 at 0.37 THz, 372 at 0.39 THz, and 504 at 0.43 THz, and the corresponding extinction ratios are 23.5, 35.6, and 14.5, respectively, for the dual micro-ring waveguide with $g = 18\,\mu$m. Although the transmissions of the both waveguides are almost the same, the bigger the g, the easier the fabrication of the waveguides. Furthermore, the transmissions of dual and single ring WGMR waveguides with the same g were also calculated. In the lower Fig. 1(b), the black and pink curves show the transmissions of single and dual micro-ring WGMR waveguides with the same gap value of 18 μm. Obviously, the dual micro-ring WGMR waveguide has obvious advantages in the Q and extinction ratio compared with the single ones with the same g. Therefore, the dual micro-ring WGMR was selected to fabricate in the following experiment. In addition, the designed both waveguides have good resonance characteristics in the whole calculated THz wave band.

The electric intensity distribution of the waveguide was calculated to further investigate the resonance characteristics and high coupling efficiency of the dual micro-ring WGMR waveguide. The WGMR cross-sectional electric field intensity distribution for various frequencies at around 0.390 THz is shown in Figs. 1(c)–1(e). When the frequency is 0.3895 THz, part of the energy is coupled with the micro-ring, and the electric field intensity in the micro-ring is equivalent to that of the incident signal. When the frequency is 0.3900 THz, the signal and micro-ring resonate strongly, most of the energy enters the micro-rings, and the electric field intensity is 2.4 times that of the incident signal. When the frequency is 0.3921 THz, the signal does not resonate with the micro-ring, and most of the energy does not interact with the micro-rings. Instead, it is directly output through the straight waveguide. Thus, the micro-rings have a strong resonance effect on the signal at a specific frequency, and the dual micro-ring structure significantly enhances the resonance effect on the THz.

A gradual taper was used to reduce the coupling loss of the WGMR waveguide. The taper size was limited by the dimension of the WGMR, its height and width were fixed, and the gradient was carried out on the width w, as shown in Fig. 2(a). The THz signal was coupled to the dielectric waveguide through a standard rectangular metal waveguide. The type of rectangular metal waveguide was WR2.2, the height was 570 μm, and the width was 285 μm. The calculated reflectivity of the waveguide ports was obtained through parameter scanning of the included angle parameters of the taper, as shown in Fig. 2(b). The results show that in most cases, the port reflectivity was less than 0.05 when $\theta = 9.5°$. Additionally, the coupling loss between the metal waveguide and chip was only 0.22 dB, indicating that the coupling efficiency was highest under this parameter. When there was no taper structure, the port reflectivity was greater than 0.5, which proves that it is necessary to add a taper structure to the WGMR.

According to the optimized structure and parameters described above, the dual micro-ring WGMR waveguide chips were prepared in

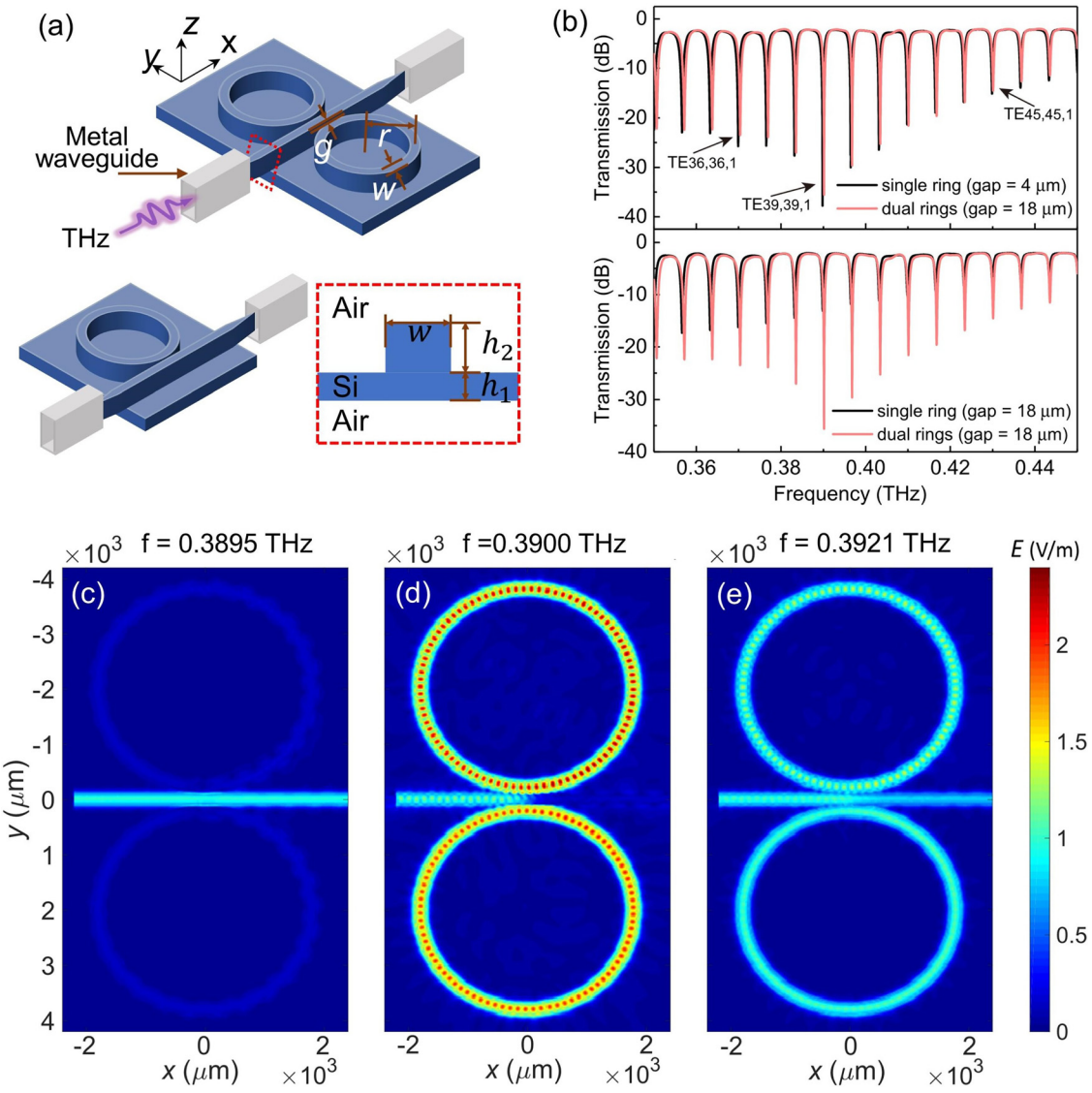

FIG. 1. (a) Designs of single micro-ring and dual micro-ring WGMR waveguide. The red framed image in the lower right corner represents a cross section. (b) Comparison results of transmission amplitude between single and dual with the same size micro-ring WGMR waveguides. The upper half of the figure shows the comparison results of the single ring WGMR when the gap is 4 μm and the dual rings WGMR when the gap is 18 μm, and the lower half of the figure shows the comparison results of the single and dual rings WGMR when the gap is 18 μm. The WGMR cross-sectional electric field strength map at (c) 0.3895, (d) 0.3900, and (e) 0.3921 THz. The three figures are the electric field strength on the XY plane with the same height in the Z direction. In the calculations, the complex refractive index of silicon is $3.4174 + 0.0018i$.

batches using a deep silicon etching micro-fabrication process on an HRFZ-Si ($\rho > 10\,000\ \Omega$ cm) platform. The THz wavelength is on the order of 100 μm compared with visible and infrared light, which reduces the ultra-high precision machining requirements of the resonator structure. The actual sizes of the fabricated WGMR waveguide are shown in Fig. 3 and were measured as follows: the radius was 1832 μm, gap size was 16 μm, length of the tapered structure was 1340 μm, and angle of the gradual taper was approximately 8.9°, which were close to the parameters calculated above.

In the experimental demonstration, the terahertz network analyzer (Ceyear 3672E) developed by the 41st Research Institute of CETC was used to measure the amplitude and phase of the reflection (S11) and transmission (S21) coefficients of the WGMR waveguide. The WGMR waveguide was micro-assembled and encapsulated in the standard WR2.2 waveguide module, as shown in Fig. 3(d). During the experiment, the packaged WGMR waveguide was connected with the network analyzer through the standard waveguide flange (WR2.2), that is, waveguide coupling, as shown in Fig. 3(e). The package with a standard rectangular metal waveguide was designed to test the resonance feature and improve the anti-interference ability of the WGMR, which packaged the chip in a box with a WR2.2 standard waveguide, as shown in Fig. 3(d). The phenomenon of mode splitting caused by

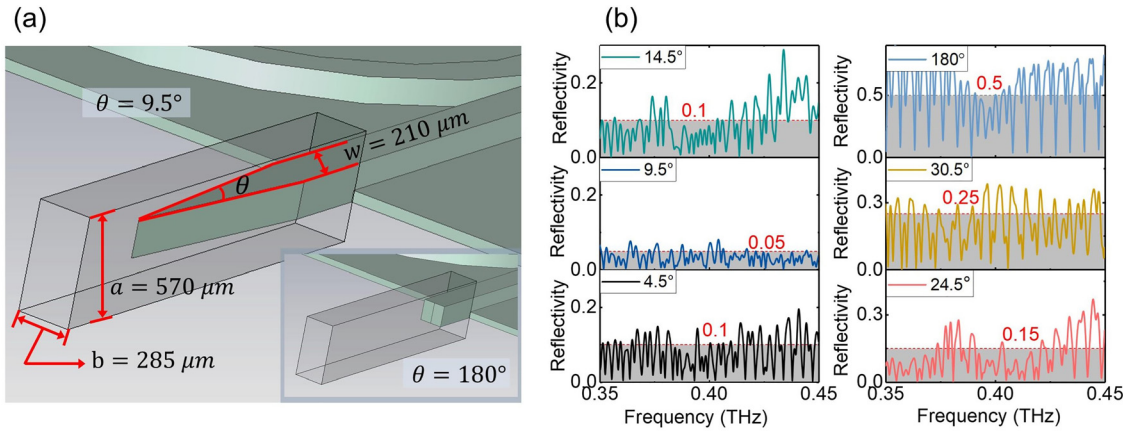

FIG. 2. (a) Gradual taper structure of the waveguide chip. The taper angle parameter shown is 9.5°, and the taper angle parameter in the lower right corner is 180°, i.e., without taper structure. (b) Results of the taper effect on coupling efficiency, simulating the waveguide ports reflectivity under different angles of the taper from 4.5° to 180°.

external impurities falling into the mode volume of the WGM could also be avoided.

The measured amplitude and phase of the transmission of the WGMR waveguide chip are shown in Fig. 4(a), demonstrating that the test results are aligned with the calculated results. The extinction ratio of all the resonant peaks was almost greater than 20 dB. The WGM coupling strength can be concluded from the change of phase and extinction ratio of the resonance peaks. When the phase produces a π jump, the coupling state is a critical coupling; the internal losses equal the coupling losses, as seen in Fig. 4(c). When the change of phase is not monotonous and less than π, the coupling state is under-coupling, as shown in Fig. 4(d). The measured extinction ratios were 32 and 18 dB, and Q factors were 385 at 0.39 THz and 502 at 0.43 THz for the TE39 and TE45 modes, respectively. The insertion loss of the packaged WGMR chip was very small, only 2.6 dB overall, as shown in Fig. 4(a), which is much lower than the 6 dB loss reported in the existing literature.[33] The measured reflectivity of the packaged waveguide was less than −13 dB in the 0.360 to 0.440 THz range, as shown in Fig. 4(b), and it indicates that the angle-optimized gradual taper can transfer the THz signals from a rectangular metal waveguide to a dielectric waveguide efficiently. All these measured results are agreed well with the calculated ones, and it fully shows the accuracy of our waveguide design and lays a solid foundation for our future development of larger array waveguide devices. Here, the Q factors of the WGMR waveguide are low compared with the counterparts in the optical band, but within the normal range in the THz region. The main reasons are as follows: on the one hand, the radius size of the dual micro-ring is only 1832 μm, which is far small than the reported ones,[27–31] and it means the bending loss will be relatively large. On the other hand, the Q-factor is limited by the surface roughness from the etching process and the intrinsic loss of materials. Some photoresist contaminants and damage defects were observed in the waveguide chip. In addition, in the experiment, the transmission loss of the waveguide is about 2.6 dB in the whole measurement range, including the coupling loss of the metal waveguide and taper and the dielectric loss of the WGMR. Next, we will further reduce the loss and improve the resonant Q value of

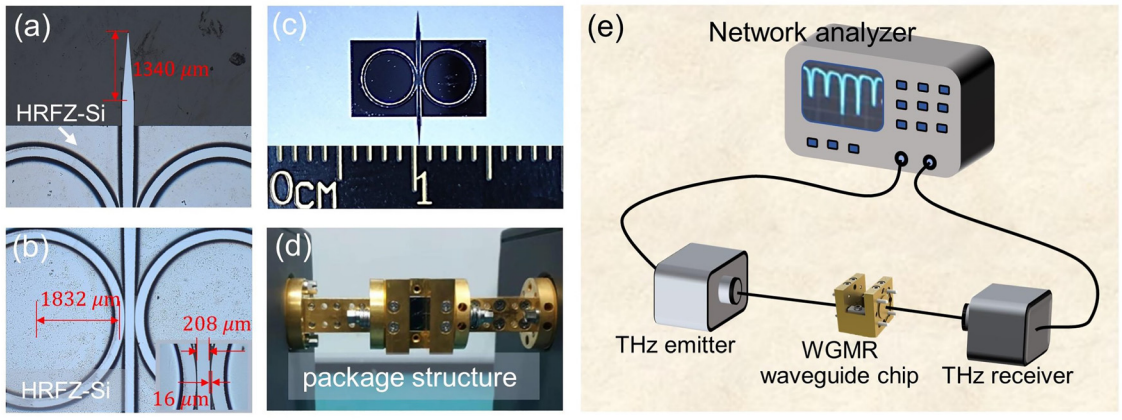

FIG. 3. (a) Gradual taper of the waveguide chip with measured angle $\theta = 8.9°$. (b) Detailed photo of the gap g, micro-ring, and gap sizes observed and measured under a microscope. $r = 1832$ μm, $g = 16$ μm, and $w = 208$ μm, and (c) photo of the WGMR waveguide chip. (d) Photo of the WGMR waveguide chip package. (e) Schematic diagram of the WGMR waveguide chip measurement system with the THz network analyzer.

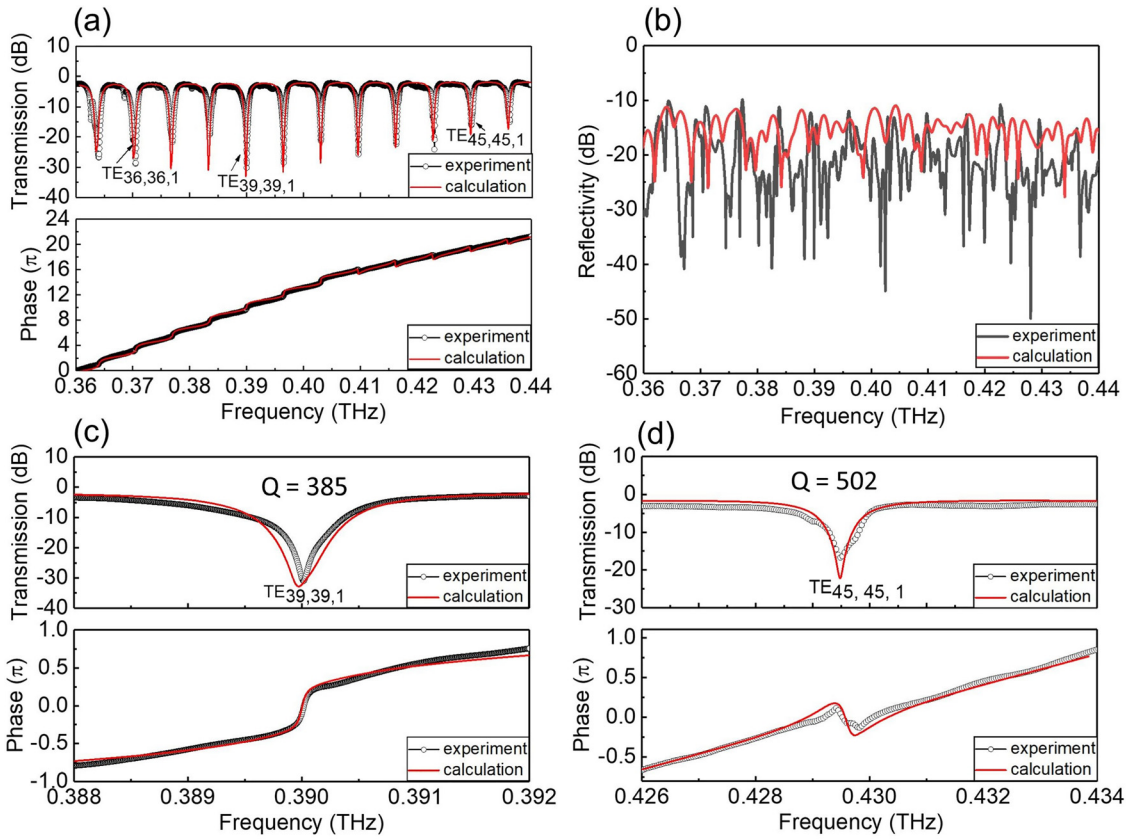

FIG. 4. Amplitude and phase results of the (a) transmission and (b) reflectivity of the WGMR waveguide. The red and black curves are the calculation and measured results of the network analyzer, respectively. (c) and (d) are the amplitude and phase results of a single resonant peak for frequency ranges of 0.3880 to 0.3920 THz and 0.4260 to 0.4340 THz, respectively. The Q-factors were calculated by Lorentz fitting the measured data in the linear coordinates.

the waveguide from the three aspects mentioned above. Obviously, if more WGMRs and I/O waveguides are added, the packaged waveguide chip here can be used in THz wireless communication systems to achieve the core functions of wavelength-division multiplexing (WDM) and filtering.[41,42]

In summary, this study proposed a THz whispering gallery mode resonator waveguide chip on a silicon platform that demonstrated high performance. The calculated and measured electromagnetic resonance characteristics were analyzed in detail and aligned well. The dual micro-ring WGMR waveguide with an operating range of 0.360 to 0.440 THz had a maximum measured extinction ratio of 32 dB at 0.390 THz, Q factor of 385, and an insertion loss of 2.6 dB. Simultaneously, a gradual silicon taper was integrated into the WGMR waveguide on the same chip to reduce the coupling loss between the metal rectangular waveguide and WGMR. The WGMR waveguide proposed in this study has favorable applications in THz communication systems and can be used for filtering and WDM. The proposed approach can also be used as a universal complex signal processing platform to integrate THz functional devices such as terahertz sources, modulators, and detectors.

The authors acknowledge the support from the National Natural Science Foundation of China (Nos. 61801209, 61521001, 61801206, and 11227904), National Key R&D Program of China (Grant Nos. 2018YFB1801504 and 2017YFA0304002), Excellent Youth Natural Science Foundation of Jiangsu Province (No. BK20200060), Priority Academic Program Development of Jiangsu Higher Education Institutions (PAPD), and Fundamental Research Funds for the Central Universities and Jiangsu Key Laboratory of Advanced Techniques for Manipulating Electromagnetic Waves. This work was supported by the 41st Research Institute of China Electronics Technology Group Corporation (CETC) for providing the test equipment.

AUTHOR DECLARATIONS

Conflict of Interests

The authors declare no conflicts of interest.

DATA AVAILABILITY

The data that support the findings of this study are available from the corresponding author upon reasonable request.

REFERENCES

[1]D. M. Mittleman, J. Appl. Phys. **122**, 230901 (2017).
[2]D. M. Mittleman, Opt. Express **26**, 9417 (2018).
[3]I. Mehdi, J. V. Siles, C. Lee, and E. Schlecht, Proc. IEEE **105**, 990 (2017).

[4]K. Sengupta, T. Nagatsuma, and D. M. Mittleman, Nat. Electron. **1**, 622 (2018).
[5]T. Nagatsuma, G. Ducournau, and C. C. Renaud, Nat. Photonics **10**, 371 (2016).
[6]K. Tsuruda, M. Fujita, and T. Nagatsuma, Opt. Express **23**, 31977 (2015).
[7]G. Chattopadhyay, T. Reck, C. Lee, and C. Jung-Kubiak, Proc. IEEE **105**, 1139 (2017).
[8]W. Withayachumnankul, M. Fujita, and T. Nagatsuma, Adv. Opt. Mater. **6**, 1800401 (2018).
[9]W. Withayachumnankul, R. Yamada, M. Fujita, and T. Nagatsuma, APL Photonics **3**, 051707 (2018).
[10]W. J. Gao, W. Lee, X. Yu, M. Fujita, T. Nagatsuma, C. Fumeaux, and W. Withayachumnankul, IEEE Trans. Terahertz Sci. Technol. **11**, 28 (2020).
[11]S. Yuan, L. Chen, Z. Wang, W. Deng, Z. Hou, C. Zhang, Y. Yu, X. Wu, and X. Zhang, Nat. Commun. **12**, 5570 (2021).
[12]B. Beuerle, J. Campion, U. Shah, and J. Oberhammer, IEEE Trans. Terahertz Sci. Technol. **8**, 248 (2018).
[13]M. Mittendorff, S. Li, and T. E. Murphy, ACS Photonics **4**, 316 (2017).
[14]X. Yu, M. Sugeta, Y. Yamagami, M. Fujita, and T. Nagatsuma, Appl. Phys. Express **12**, 012005 (2019).
[15]H. Li, M. X. Low, R. T. Ako, M. Bhaskaran, S. Sriram, W. Withayachumnankul, B. T. Kuhlmey, and S. Atakaramians, Adv. Mater. Technol. **5**, 2000117 (2020).
[16]K. Wang and D. M. Mittleman, Nature **432**, 376 (2004).
[17]G. Gallot, S. P. Jamison, R. W. McGowan, and D. Grischkowsky, J. Opt. Soc. Am. B **17**, 851 (2000).
[18]S. Atakaramians, S. Afshar V, T. M. Monro, and D. Abbott, Adv. Opt. Photonics **5**, 169 (2013).
[19]M. S. Islam, C. M. B. Cordeiro, M. A. R. Franco, J. Sultana, A. L. S. Cruz, and D. Abbott, Opt. Express **28**, 16089 (2020).
[20]A. Chiasera, Y. Dumeige, P. Féron, M. Ferrari, Y. Jestin, G. Nunzi Conti, S. Pelli, S. Soria, and G. C. Righini, Laser Photonics Rev. **4**, 457 (2010).
[21]C. Grivas, C. Li, P. Andreakou, P. Wang, M. Ding, G. Brambilla, L. Manna, and P. Lagoudakis, Nat. Commun. **4**, 2376 (2013).
[22]L. He, Ş. K. Özdemir, J. Zhu, W. Kim, and L. Yang, Nat. Nanotechnol. **6**, 428 (2011).
[23]J. Liao and L. Yang, Light Sci. Appl. **10**, 32 (2021).
[24]N. Toropov, G. Cabello, M. P. Serrano, R. R. Gutha, M. Rafti, and F. Vollmer, Light Sci. Appl. **10**, 42 (2021).
[25]J. Zhang and D. Grischkowsky, J. Opt. Soc. Am. B **20**, 1894 (2003).
[26]S. Yuan, L. Chen, Z. Wang, R. Wang, X. Wu, and X. Zhang, Opt. Lett. **44**, 2020 (2019).
[27]Z. Wang, S. Yuan, G. Dong, R. Wang, L. Chen, X. Wu, and X. Zhang, Opt. Lett. **44**, 2835 (2019).
[28]S. Yuan, L. Chen, Z. Wang, R. Wang, X. Wu, and X. Zhang, Appl. Phys. Lett. **115**, 201102 (2019).
[29]D. W. Vogt and R. Leonhardt, APL Photonics **3**, 051702 (2018).
[30]D. W. Vogt and R. Leonhardt, Optica **4**, 809 (2017).
[31]D. W. Vogt, A. H. Jones, T. A. Haase, and R. Leonhardt, Photonics Res. **8**, 1183 (2020).
[32]C. Mathai, R. Jain, V. G. Achanta, S. P. Duttagupta, D. Ghindani, N. R. Joshi, R. Pinto, and S. S. Prabhu, Opt. Lett. **43**, 5383 (2018).
[33]J. Xie, X. Zhu, X. Zang, Q. Cheng, L. Chen, and Y. Zhu, Opt. Mater. Express **8**, 50 (2018).
[34]S. S. Prabhu and V. G. Achanta, Adv. Opt. Mater. **8**, 1900973 (2020).
[35]J. Liang, W. Gao, H. Lees, and W. Withayachumnankul, IEEE Antennas Wireless Propag. Lett. (published online, 2021).
[36]Y. Yang, Y. Yamagami, X. Yu, P. Pitchappa, J. Webber, B. Zhang, M. Fujita, T. Nagatsuma, and R. Singh, Nat. Photonics **14**, 446 (2020).
[37]M. Fujita and T. Nagatsuma, "Photonic crystal technology for terahertz system integration," in *Terahertz Physics, Devices, and Systems X: Advanced Applications in Industry and Defense*, (Society of Photo-Optical Instrumentation Engineers, 2016), Vol. 9856, p. 98560.
[38]C. Damm, H. G. L. Schwefel, F. Sedlmeir, H. Hartnagel, S. Preu, and C. Weickhmann, in *Semiconductor TeraHertz Technology* (John Wiley & Sons, Ltd, 2015), pp. 340–382.
[39]S. Yang, Y. Wang, and H. D. Sun, Adv. Opt. Mater. **3**, 1136 (2015).
[40]J. Dai, J. Zhang, W. Zhang, and D. Grischkowsky, J. Opt. Soc. Am. B **21**, 1379 (2004).
[41]N. J. Karl, R. W. McKinney, Y. Monnai, R. Mendis, and D. M. Mittleman, Nat. Photonics **9**, 717 (2015).
[42]J. Ma, N. J. Karl, S. Bretin, G. Ducournau, and D. M. Mittleman, Nat. Commun. **8**, 729 (2017).